Optimizing Tris(2-Carboxyethyl)phosphine and Mercaptohexanol Concentrations for Thiolated Oligonucleotide Immobilization on Platinum Electrodes in Microfluidic Platforms

Choayb Omar, Martina Freisa, Hiu Mun Man, Djamila Kechkeche, Thi Hong Nhung Dinh, Anne-Marie Haghiri-Gosnet, Isabelle Le Potier, Jean Gamby

▶ **To cite this version:**

Choayb Omar, Martina Freisa, Hiu Mun Man, Djamila Kechkeche, Thi Hong Nhung Dinh, et al.. Optimizing Tris(2-Carboxyethyl)phosphine and Mercaptohexanol Concentrations for Thiolated Oligonucleotide Immobilization on Platinum Electrodes in Microfluidic Platforms. Langmuir, 2024, 40 (50), pp.26616-26625. 10.1021/acs.langmuir.4c03566 . hal-04856155

HAL Id: hal-04856155
https://hal.science/hal-04856155v1

Submitted on 26 Dec 2024

HAL is a multi-disciplinary open access archive for the deposit and dissemination of scientific research documents, whether they are published or not. The documents may come from teaching and research institutions in France or abroad, or from public or private research centers.

L'archive ouverte pluridisciplinaire **HAL**, est destinée au dépôt et à la diffusion de documents scientifiques de niveau recherche, publiés ou non, émanant des établissements d'enseignement et de recherche français ou étrangers, des laboratoires publics ou privés.

Distributed under a Creative Commons Attribution 4.0 International License

Optimizing tris(2-carboxyethyl) phosphine and mercaptohexanol concentrations for thiolated oligonucleotide immobilization on platinum electrodes in microfluidic platforms

Choayb Omar[1,⊥], Martina Freisa[1,⊥], Hiu Mun Man[1], Djamila Kechkeche[1], Thi Hong Nhung Dinh[1], Anne-Marie Haghiri-Gosnet[1], Isabelle Le Potier[1], and Jean Gamby[1,*]

[1] *Université Paris-Saclay, CNRS, Centre de Nanosciences et de Nanotechnologies (C2N), 91120, Palaiseau, France*

*** Corresponding authors:** jean.gamby@cnrs.fr

[⊥] Both authors have equally contributed to this work

Abstract

In this study, we propose a strategy to explore the impact of the proportion of tris(2-carboxyethyl)phosphine (TCEP) and 6-mercaptohexanol (MCH) on the efficiency of oligonucleotide functionalization on PDMS microfluidic channels equipped with pairs of homemade microfabricated platinum microelectrodes. We identified an optimal concentration of these compounds that enables effective orientation and distribution of probes, thereby facilitating subsequent target hybridization. The experiment included optimizing sample injection into microfluidic channels. We used TCEP as a reducing agent to help the DNA probes adhere to the channel electrode better. This stopped the formation of disulfide bonds during the probe immobilization step. We found the optimal TCEP/MCH mixture ratio (5 mM TCEP and 50 mM MCH), which led to a more uniform distribution and orientation of the DNA probes on the platinum electrode. These optimized conditions resulted in a more compact DNA monolayer and enhanced detection capabilities. The biosensor's performance was evaluated by the detection of the hybridization of complementary DNA sequences in the presence of equimolar $Fe(CN)_6^{3-}$ / $Fe(CN)_6^{4-}$. The detection of the synthetic GP8 resistance gene is facilitated by a measurable decrease in the electron transfer rate, which is directly proportional to its concentration. Under the optimized conditions, the DNA biosensor showed excellent sensitivity (with a detection limit of 10^{-17} M) and high specificity when tested against non-complementary DNA strands.

Keywords: tris(2-carboxyethyl) phosphine; 6-mercaptohexanol; platinum; microfluidics; nucleic acids, DNA biosensor

Introduction

In recent years, different types of electrochemical biosensors based on nucleic acid recognition have been developed [1–3]. The main advantages of electrochemical DNA biosensors over other types of DNA sensors include ease of miniaturization, the compatibility with microfabrication techniques, simple instrumentation, remarkable sensitivity and selectivity, rapid response time, ease of use, portability, cost-effectiveness and low power requirements [4–6]. In electrochemistry, to detect target nucleic acid sequences, the biological receptor is generally the probe DNA sequence, which is complementary to the target sequence[7,8]. The most common transducers are modified electrodes. Electrochemical biosensors can be classified into two categories depending on the electrode configurations: 1) the three-electrode system consisting of the working, reference and auxiliary electrodes and 2) the two-electrode system composed of the working and reference electrodes. The working electrodes (WE) are ideally made of polarizable materials, commonly including noble metals such as gold, palladium, or platinum, as well as carbon-based materials. Among the different DNA immobilization methods, the direct adsorption method is the simplest and minimizes the use of chemical reagents. The negatively charged phosphate backbone of DNA allows DNA to be immobilized through interactions with a cationic polyelectrolyte [4]. These substances generally include chitosan, cationic polymer films, as well as graphene oxide/Fe_3O_4 nanocomposites and glutaraldehyde. Additionally, the application of a positive potential across electrodes has been reported to improve the stability of the immobilized DNA probes. Velusamy *et al.*[9] reported an electrochemical DNA biosensor for the detection of *Bacillus cereus* DNA. The gold electrode surface was modified with polypyrrole (PPy) to immobilize DNA, and then a fixed potential of 0.8 V for 600 s was applied to improve the immobilization efficiency and stability. In addition to the adsorption method, covalent bonding is another common method for immobilizing DNA on electrode surfaces. Tabrizi *et al.*[10] developed an electrochemical DNA biosensor based on nanoporous glassy

carbon electrodes to detect Salmonella DNA sequences. The amine-modified probe DNA (-NH_2) was first covalently linked with the carboxylic group (-COOH) on the nano-porous glassy carbon electrodes. Then, the target DNA hybridized with the probe DNA. Furthermore, self-assembly is another common covalent bonding method for DNA immobilization on the electrode surface[11,12]. Horny *et al.*[13] developed an electrochemical DNA biosensor to detect the DNA target that mimics micro-ribonucleic acid 122 (miRNA122) specific for early liver injury. The developed biosensor was composed of a pair of gold electrodes: a large counter electrode and a small working electrode. The probe DNA was modified at the 5' end with a thiol function for the direct immobilization on gold via Au-S bonds. Then, the target DNA was incubated with the probe DNA for 30 minutes for hybridization. The sensor demonstrated excellent sensitivity, with the detection limit down to 10^{-18} M. The specificity of this biosensor was further improved by Poujouly *et al.*[14] thanks to the addition of methylene blue in the electrolyte. This addition allows the hybridization of the mismatched DNA to be distinguished from the perfect-matched complementary DNA, regardless of the mismatch location in the DNA strand. Although gold is typically considered chemically inert, the continuous loss of thiol-terminated DNA probes suggests that the stability of this bond is lower than previously assumed, which can lead to issues with the reproducibility of results [15]. Lee *et al.*[15] investigated the instability of gold electrodes in the context of electrochemical DNA detection using the ferri/ferrocyanide redox couple. They observed a progressive decrease in measured resistance, which they attributed to the loss of DNA probes, suggesting that the integrity of the gold surface deteriorates over time. The study links the decrease in charge transfer resistance during repeated measurements to the instability of the gold-thiol bond.

Platinum presents an interesting alternative to gold as it is much more electrochemically stable and less prone to non-specific adsorptions, particularly in experiments involving complex biological environments[16,17]. Despite these advantages over gold, few articles focus on self-

assembled monolayers (SAMs) on platinum. While the Au-S bonds reaction occurs spontaneously, one of the limitations of platinum is linked to the fact that the DNA probes immobilized on the platinum surface are likely poorly oriented due to a strong affinity between the Pt surface and the oligonucleotide backbone [16]. These observations have motivated our current work in fabricating devices featuring platinum microbands and adapting the existing tris(2-carboxyethyl)phosphine (TCEP) as reducing agent TCEP on supramolecular protein assembly[18,19]. To this goal, thiol-modified DNA and 6-mercaptohexanol (MCH) were mixed in the presence of TCEP to optimize the orientation and self-organization of DNA probe strands, thereby enabling efficient detection of specific targets.

Experimental Section

Chemicals and electrochemical protocols

Sodium chloride, potassium hydroxide, potassium hexacyanoferrate (III), and potassium hexacyanoferrate (II) trihydrate were acquired from Sigma Aldrich (France) along with 6-mercaptohexanol (MCH). Tris(2-carboxyethyl) phosphine (TCEP), was acquired from Thermo Fisher Scientific (France). The DNA probes and targets (See Table 1), each comprising 21 nucleotides, were obtained from Eurogentec and purified via reverse-phase HPLC by the supplier. The probes, labeled with a 5' (-SH) C6 modification, mirrored the complementary target sequences.

Briefly, the selected sequences in this work are resistance genes *i.e.* a portion of DNA that allows the bacteria to acquire a defense mechanism against antimicrobials. Resistance genes vary depending on their target in order to block the process of action of antibiotics. They most often encode enzymes capable of inactivating, and more rarely of modifying, the affinity of antibiotics for their target [20]. In this article, we tested the TCEP/ MCH protocols with the detection of antibiotic resistance genes which will be used for ongoing works about the molecular diagnosis of antibiotic resistance in *Escherichia coli*, the main bacterium responsible for severe sepsis. Table 1 below presents the sequences mimicking antibiotic resistance genes used throughout this work. We used the DNA probe corresponding to ***Probe GP8***, while the ***Target GP8*** corresponds to the complementary sequence (denoted as C in Table 1). To study the specificity of the developed biosensors, we have used a non-complementary (NC in the Table 1 below) strand called ***Target GP2***. In our study, we aimed to detect the CTX-M genes from groups 2 and 8 due to their prevalence and clinical significance[21,22]. Extended-spectrum β-lactamases (ESBLs) of the CTX-M family have become a major factor contributing to antibiotic resistance globally, particularly among Enterobacteriaceae. Although CTX-M groups 2 and 8 are encountered less frequently than others, they are still associated with resistance to

β-lactam antibiotics. Therefore, their detection is essential for effectively managing antimicrobial resistance, especially in severe infections like sepsis, where prompt and appropriate treatment is crucial.

Table 1. Nucleic acid sequences used in this work.

	Nucleotide sequence
Probe GP8	5′-thiol C6*-GCG-GCG-CTG-GAG-AAA-AGC-AGC-GG-3′
Target GP8 (C)	3′-CGC-CGC-GAC-CTC-TTT-TCG-TCG-CC-5′
Target GP2 (NC)	3′-CAC-CCG-CTA-TTT-TGG-CCG-TCG-CC-5′

**Nomenclature for modified oligonucleotides: C6 refers to the 6-carbon spacer that separates the thiol (S-S) group and the oligonucleotide.*

For Pt-electrode functionalization, probes were immobilized using a 10^{-6} M DNA concentration in 0.5 M NaCl. Meanwhile, Pt-electrode functionalization involved a solution of 10^{-5} M probes mixed with $5 \cdot 10^{-2}$ M (optimal concentration) 6-mercaptohexanol (MCH, Sigma Aldrich) in NaCl. Immobilization of probes for Pt electrodes took place under static conditions for 2 hours. Additionally, complementary targets, diluted in 0.5 M NaCl, underwent a 30-minute hybridization process under static conditions. TCEP was mixed with the DNA probe to reduce disulfide bonds.

Microfabrication of platinum microelectrodes

The different stages of optical photolithography on glass plates, shown schematically in Figure 1, are described in detail below:

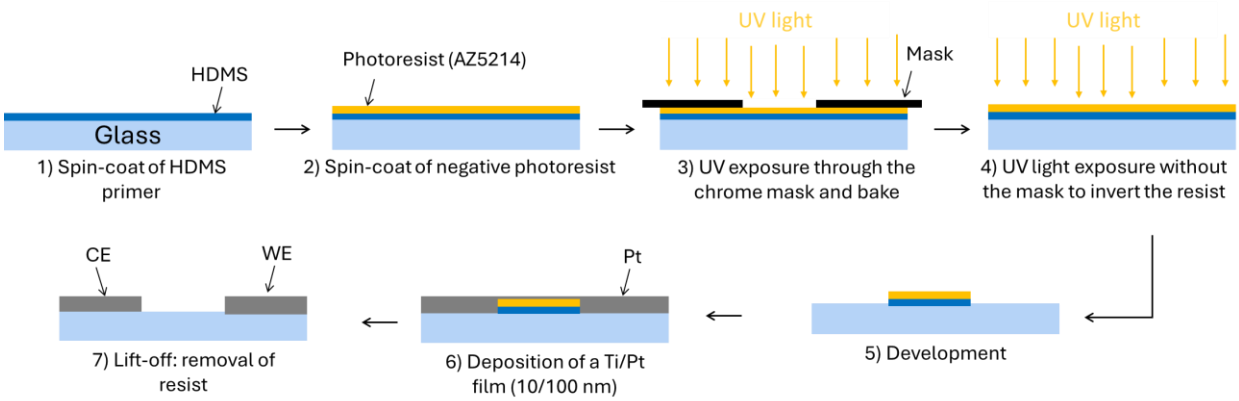

Figure 1. The different stages of microelectrode fabrication.

The first step consists of depositing a film of hexamethyldisilazane (HDMS) as a primer. This layer of HDMS is therefore spread on the substrate using a spin-coater using the following parameters: speed = 4000 rpm; acceleration = 2000 rpm s^{-1} and time = 30 s (see step 1 in Figure 1). The second step is the deposition of an AZ5214 photosensitive resin film on the glass substrate by spin coating using the previously mentioned parameters (see step 2 in Figure 1). The AZ5214 resin is a reversible photosensitive resin, the polarity of which can be changed after annealing or a second UV exposure. For our application, we use this reversible resin which allows us to produce patterns with a thickness equal to 1.4 µm. The glass substrate is then heated on a horizontal heating plate at 110°C for 1 min in order to evaporate the solvents present in the resin to increase the adhesion of the resin and to be able to bring it into contact with the mask during the next step. The third step consists of illuminating the resin-coated glass substrate with a UV source through the mask (in the hard contact mode) for 5 seconds using an "MJB4" UV aligner (see step 3 of Figure 1). This aligner transmits UV radiation with a well-defined range of wavelengths (λ= 365 – 405 nm, lamp power = 7 mW cm^{-2}) through a filter placed between the mercury lamp and the sample to be exposed. This step allows us to reproduce the structure of the patterns existing on the optical mask in the resin. These patterns correspond to the geometry of the electrodes which were generated with the L-edit software. The exposure step is always followed by an annealing step at 120 °C for 2 min. The resin layer then undergoes a second UV lithography step without the mask for 35 seconds, which allows the resin to be

inverted. This means that the patterns obtained during the first exposure become insoluble in the developer.

The final stage is development. The substrate is immersed in a bath which contains the metal-ion-free (MIF) developer AZ826 for 50 seconds. This liquid will selectively dissolve the resin in non-exposed areas. The substrate is then rinsed in deionized water for 2 min. Finally, the sample undergoes an O_2 plasma treatment for 30 seconds in order to remove any traces of resin at the bottom of the patterns.

Metallization and lift-off of the electrodes

In order to improve the adhesion of platinum to the glass substrate, a titanium adhesion layer was used. A Ti layer as adhesion layer, together with Pt bilayer with a thickness of 5 nm and 50 nm respectively, were deposited on the glass substrate covered of AZ5214 resin. The two layers were successively deposited by using the evaporation technique (Plassy MEB550-S metal evaporator), which involves heating the material in a vacuum chamber, allowing the produced vapor to condense on the substrate to form a thin layer with predefined thickness (see step 6 of Figure 1).

This step is always followed by a lift-off of the resin. This operation consists of putting the sample in an acetone bath for 5 min to remove the resin leaving only the Ti/Pt layer on the substrate (see step 7 of Figure 1).

Fabrication of the master mold and the PDMS device

For the fabrication of the SU8 mold containing microfluidic channels for DNA solution circulation, standard photolithography and soft lithography techniques were used. The

microchannel designs were created using L-Edit software. In brief, SU-8, a negative photoresist, was spun onto a silicon wafer, exposed to UV light through a Mylar mask, and developed in SU-8 developer to form the master mold.

To fabricate the PDMS device, the base (dimethylsiloxane, dimethylvinyl-terminated, and trimethylated silica) was mixed with a curing agent (Tetrakis (trimethylsilyloxy) silane) in a 10:1 ratio. The mixture was then poured onto the SU-8 master mold and degassed under vacuum for one hour. The mold was placed in an oven at 60°C for four hours to allow the PDMS to solidify into a flexible silicone polymer. Once cured, the PDMS layer containing the microchannel pattern was carefully detached from the master mold. This PDMS part can then be used as a circulation network for fluids. In order to allow the connection of the channels, the PDMS is drilled with a 1 mm diameter punch (Reusable Rapid Punch Biopsy Kit, World Precision Instruments, France) to make holes at the inputs and outputs of the circuit.

For sealing the microfluidic chips, both the PDMS layer and a glass cover (Neyco, France) were activated using a plasma cleaner (Nanonex Ultra-100) for 30 seconds before being brought into contact to bond the PDMS chip. The chip was then baked at 60°C for at least four hours to ensure complete bonding.

In order to circulate fluids from previously drilled holes as inlets and outlets, we used smooth, biocompatible silicone tubing dedicated to biochemical applications (Platinum-cured silicone tubing, Darwin Microfluidics). To connect these pipes to our PDMS microfluidic chips, we used stainless steel connectors (Stainless steel straight PDMS couplers, Darwin Microfluidics), perfect for use with silicone microfluidic tubes. To circumvent the integration of three electrodes in miniaturized electrochemical systems, two-electrode electrochemical systems are increasingly used to facilitate connectivity with the potentiostat[23]. These systems are composed of a microelectrode as the working electrode and a large surface electrode as the counter

electrode and reference electrode [24,25]. In our configuration, the counter electrode simultaneously plays the role of pseudo-reference thanks to its large size [13]. The electrochemical sensor previously developed in our group [13,25,26], is composed of two pairs of platinum electrodes on the same channel, each pair of electrodes is composed of a large counter electrode (2 mm x 300 µm) and a small working electrode (30 µm x 300 µm = $9 \cdot 10^{-5}$ cm^2). Figure 3 shows microfluidic devices complete and ready for use.

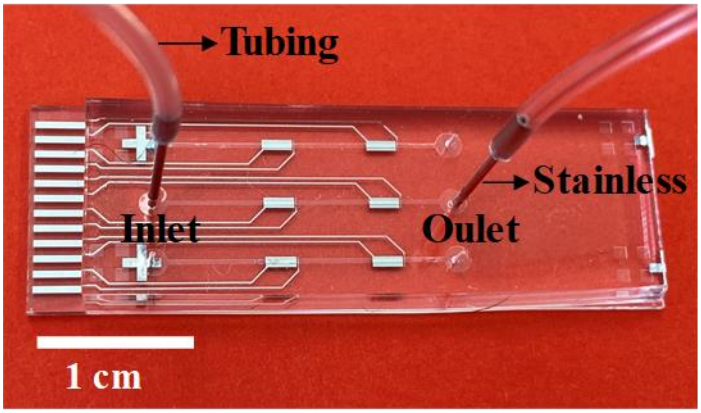

Figure 2. The fabricated microfluidic device with connectors at the inlet and outlets of fluids for electrochemical detection.

Experimental set-up

The initial step consists of inserting the chip into a printed circuit board (PCB) associated with a 3D printed support, manufactured in the laboratory, which allows the electrodes of the microfluidic chip to be connected to the potentiostat electrometer (Biologic SP-300, France). The fluidic connections are introduced, and the solutions are injected using a syringe pump (Nemesys, CETONI, Germany). Fluid leakage is tested by pumping NaCl 0.5 M in the microfluidic channel for 5 min. The experimental bench is connected to a computer with the proprietary software (EC-lab and Nemesys) to synchronize the management of flows and the acquisition of electrochemical measurements.

DNA immobilization protocols

DNA Sample pre-treatment with TCEP before use. Maintaining the probe nucleic acids in suspension for a long time can cause the formation of disulfide bridges between the thiol functions at the ends of the DNA strands. These disulfide bridges (S-S bond) are covalent bonds that form spontaneously (see Figure 3 below where the R groups represent the sequence of the oligonucleotide).

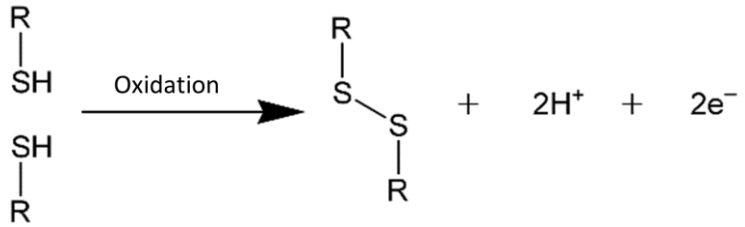

Figure 3. Formation of a disulfide bridge.

In order to avoid the creation of these bridges which will hinder the Thiol-Pt bonds and thus limit the functionalization of the DNA probes, the DNA probe solution is diluted with tris (2-carboxyethyl) phosphine (TCEP). TCEP is a reducing agent prepared and used in the form of hydrochloride salt (TCEP-HCl) with a pKa of 6.77 [27]. It is soluble in water and available as a stabilized solution at neutral pH. In our application, we used TCEP to reduce disulfide bonds as shown in Figure 4 below.

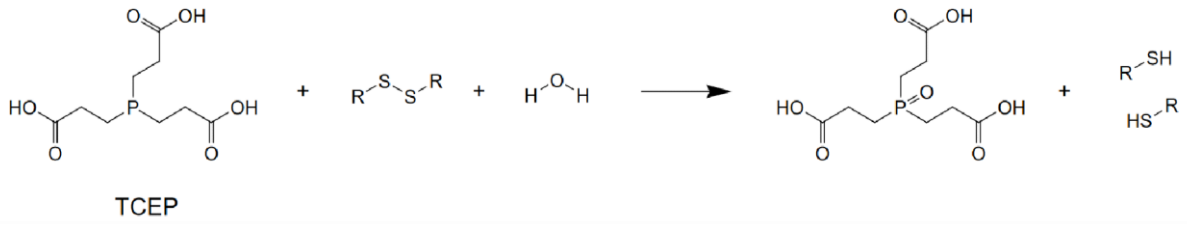

Figure 4. Reduction of organic disulfide bonds in the presence of TCEP

Functionalization of the probe sequence without MCH. The grafting of the DNA probe onto the platinum surface by chemical means is carried out by inserting a 10^{-6} M probe solution into the microfluidic channel for 2 hours at room temperature. These probes are modified with a sulfhydryl (thiol)group at the 5' end. The probe DNAs are therefore able to spontaneously bind

to the platinum atoms on the surface, allowing the spontaneous formation of a self-assembled monolayer of probe DNA[28,29] . The electrode is carefully rinsed with the electrolyte (0.5 M NaCl) in order to stabilize the probe DNA layer on the platinum electrodes.

Functionalization of the probe sequence with MCH. 2-mercaptohexanol (MCH) was used to facilitate a proper orientation of the DNA probes on the electrode surface and limit non-specific adsorption[13,29].

Indeed, MCH is a molecule which plays an important role in the orientation of immobilized DNA. It contains a thiol group which allows its adsorption to platinum electrodes vertically, and hence facilitates the hybridization of target DNAs. In this work, we mixed the probe DNA solution with an MCH solution so as to keep the concentration of probe DNAs constant (at 10^{-6} M) [30,31]. Figure 5 presents the protocol for immobilizing DNA probes with and without the introduction of MCH.

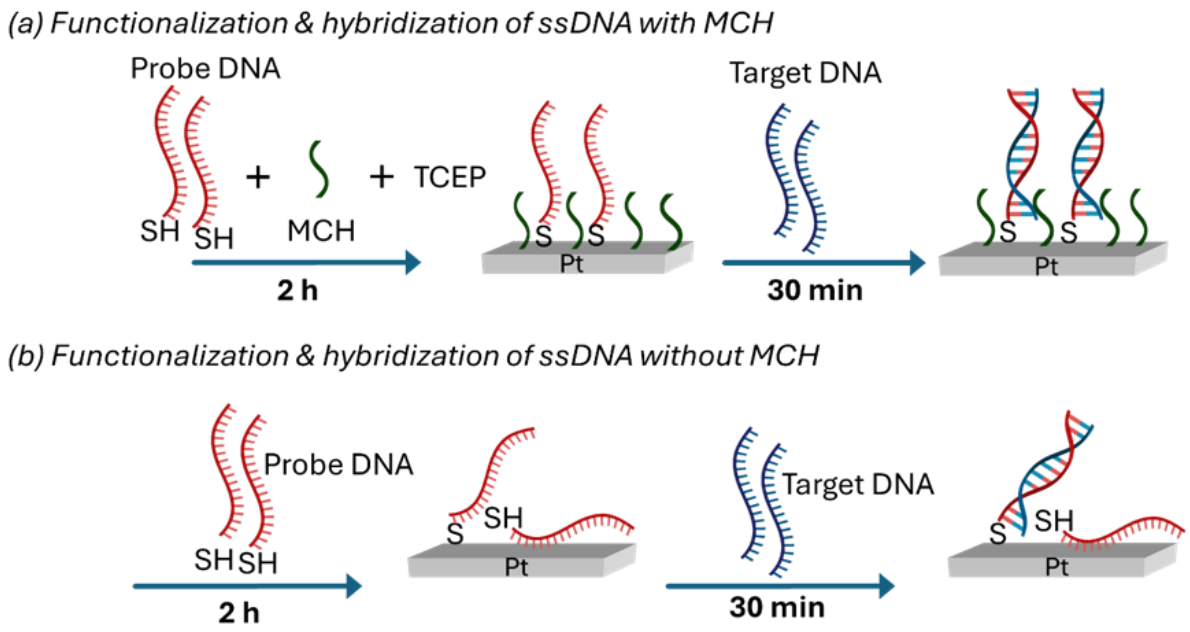

Figure 5. Effect of MCH during the stages of construction of the DNA biosensor (Pt).

Hybridization of the target sequence. The hybridization step is the actual detection of complementary DNA strands. Several solutions of complementary target DNA diluted in 0.5 M NaCl in the concentration range from 10^{-18} M up to 10^{-6} M as well as other solutions of non-complementary DNA were prepared. Hybridization of the complementary nucleic acid strand is carried out by introducing a solution of target nucleic acids into the microfluidic channel for 30 min. This procedure is repeated regardless of the procedure used for the functionalization of the probes.

Results and discussions

We used the ferrocyanide/ ferricyanide ($[Fe(CN)_6^{3-}]$ / $[Fe(CN)_6^{4-}]$) as fast kinetic redox couple in the electrolyte solution for which Equation (l) is expressed as follows:

$$[Fe(CN)_6^{3-}] + e^- = [Fe(CN)_6^{4-}] \qquad (1)$$

Figure 6 shows the cyclic voltammograms of bare platinum electrode (black curves) in ferri-/ferro-cyanide containing 0.5 M NaCl at a flow rate of 0.5 µL s^{-1}. The oxidized and reduced forms of the redox couple are used at the same concentration of 20 mM allowing us to obtain symmetrical voltammograms for oxidation and reduction. A slight asymmetry of the current levels at the diffusion plateaus can be observed due to the difference between the diffusion coefficients of ferricyanide and ferrocyanide[32]. Following the characterization of bare Pt electrode, DNA probe (without the addition of TCEP) is immobilized on the bare electrode and a decrease in absolute current can be observed as shown in Figure 6a. The absolute current decreased from 4100 nA to 2500 nA, which is as expected. As the negative charge of the probe DNA layer prevents diffusion of the redox probe in solution toward the electrode by electrostatic repulsion [33]. On the other hand, as we recently demonstrated [34], the monolayer does not perfectly cover the surface of the electrode, the redox reporter can therefore diffuse through

imperfections such as defects or holes. The evolution of the measured current therefore depends on a change in mass transport between a bare surface and a surface assimilated to a network of holes which generates a non-linearity of mass transport. Indeed, after each step: functionalization by probes then hybridization with complementary target sequences, the DNA monolayer on the electrode becomes more compact, increasing the surface coverage and correspondingly reducing the size of the available holes for the diffusion of redox probes. Thus, the measured current diminishes progressively as the holes fill up [34]. The difference in measured current is examined here for the detection of DNA hybridization.

Interestingly. the current of DNA probe was not diminishing consistently (vs. bare electrode) ***without*** the addition of TCEP. We present in Figure 6b a second case of DNA probe immobilization on platinum electrodes. In this case, no variation between the CVs of the DNA probe-immobilized electrode and the bare electrode can be observed. A further immobilization of DNA (mixed with the reducing agent TCEP) showed a decrease in absolute current (blue curve in Figure 6b). We have noticed that without the addition of TCEP, the probe current is not stable throughout the duration of experiment. This could be attributed to the fact that the DNA probes are not well organized and orientated on the Pt surface, the immobilized DNA could easily unbind under constant fluidic flow. We have therefore decided to add TCEP to DNA probes systematically in the following work in order to increase the stability of the current signals measured and the robustness of the protocol.

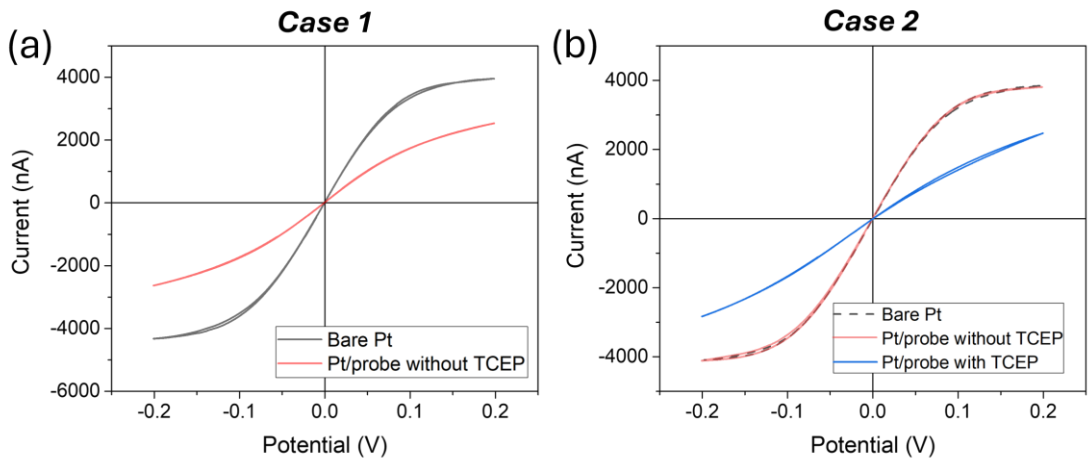

Figure 6. Cyclic voltammograms showing the effect of DNA probe immobilization with and without TCEP in a solution of 20 mM ferri/ferrocyanide containing 0.5 M NaCl at platinum microfluidic devices. (a) Case 1: bare Pt electrode (black curve), and after the immobilization of probe DNA without TCEP (red curve). (b) Case 2: bare Pt electrode (black dashed curve), after the immobilization of probe DNA without TCEP (red curve), and after the immobilization of probe DNA with TCEP.

Determination of TCEP optimal concentration for DNA Probe immobilization on Pt

As mentioned previously, it is necessary to prevent the formation of disulfide bridges which limits the adsorption of the probes. To optimize the concentration of TCEP, we prepared several DNA solutions by adding TCEP at different concentrations ranging from 0.01 mM up to 100 mM (Figure 7). These solutions are introduced into the microfluidic channel according to the protocol defined previously. The influence of increasing concentrations of TCEP from 0.01 to 100 mM mixed with the same concentration of probe DNA on the surface coverage rate (θ) is given by Equation (2) and is illustrated in Figure 7 (we mixed 10 µL of the TCEP solution in 90 µL of the 10^{-5} M probe DNA solution to obtain a final 10^{-6} M probe DNA solution). In practice, the surface coverage rate corresponds to the plot of the normalization between I_{ss}

(DNA probe current) and I_{bare} (initial current) divided by I_{bare}. The variation in the rate θ reaches a plateau which indicates the saturation of the available SH groups thanks to the reduction of disulfide bridges (presence of TCEP) for grafting. As illustrated in Figure 7, the active surface, that is to say the surface not occupied by the DNA-SH probes (ligand) is accessible for the electroactive redox couple. In this case, the surface fraction of the platinum microelectrode grafted with ligands can be estimated as follows:

$$\theta = 1 - \frac{I_{ss}}{I_{bare}} \qquad (2)$$

The experimental variation of the θ is plotted in Figure 7 using Equation (3) and the experimental curve is fitted with the Hill-Langmuir law[35], as follows:

$$\theta = \frac{1}{1+\left(\frac{K_A}{[TCEP]}\right)^n} \qquad (3)$$

where K_A is the concentration of TCEP which produces a half-maximal response (half occupancy), and n represents the Hill coefficient linked to the degree of cooperativity between the first DNA probes and the following ones throughout the functionalization step of the probe in the presence of TCEP: if $n < 1$, cooperativity decreases, if $n = 1$, cooperativity is independent, if $n > 1$, cooperativity increases.

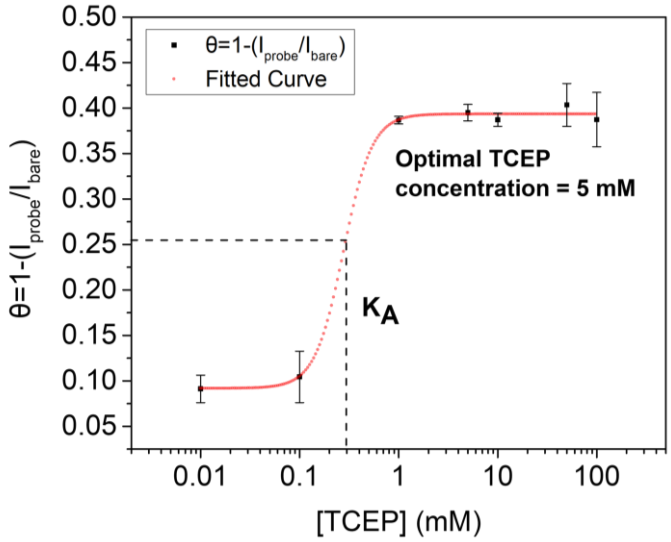

Figure 7. Effect of TCEP on the functionalization of DNA probes. Experimental evolution of the surface grafting rate simulated with the Hill-Langmuir isotherm according to Equation (3) where the parameters K_A, n and θ_{max} were determined to be (0.28 ± 0.07) mM, (2 .99 ± 0.69) and (0.393 ± 0.004), respectively.

The result of the fit using Equation (3) is shown in Figure 7. The found values of K_A and n are (0.28 ± 0.07) mM and (2.99 ± 0.69), respectively. This last value confirms a strong cooperativity between DNA probes during the immobilization procedure in the presence of TCEP. The plateau is observed at θ_{max} = 0.393 ± 0.004 for the high concentration domain (1-100 mM) and highlights that the total of adsorption sites (available during functionalization) on platinum microelectrode is reached and only represents 39.3% of the active surface of the microelectrode.

The maximum surface covered by the probes is therefore estimated at $A_{max} = 3.54 \cdot 10^{-5}$ cm^2 taking into account the fact that the working electrode surface (S_{WE}) is theoretically $9 \cdot 10^{-5}$ cm^2. The section occupied by a probe can be modeled as a disk with a radius of 1 nm corresponding to an occupied surface area of probe DNA = $3.14 \cdot 10^{-14}$ cm^2 per molecule. The maximum number, N_{max}, of grafted DNA is the ratio between A_{max} and A_{ssDNA}, (equal to $1.13 \cdot 10^9$ molecules), and the binding site density is calculated with the ratio between N_{max} and S_{WE},

(equal to $1.25 \cdot 10^{13}$ molecules.cm^{-2}). This last value is consistent with the maximum quantity of DNA fixed on a surface in the literature [13,30,31,36]. We have therefor chosen 5 mM as the optimal concentration for TCEP in the following experiments.

Determination of MCH optimal concentration for DNA Probe immobilization on Pt

Several concentrations of MCH were tested, specifically 10^{-1} M, 10^{-2} M, $2.5 \cdot 10^{-2}$ M and $5 \cdot 10^{-2}$ M, while maintaining TCEP at a concentration of 5 mM to determine the optimal MCH concentration. In Equation (4), normalization of the hybridization current is based on subtracting the probe current, I_{ss}, from the absolute target current, I_{ds}, divided by the probe current, I_{ss}:

$$I_{norm} = \frac{|I_{ss} - I_{ds}|}{|I_{ss}|} \qquad (4)$$

The calibration curves corresponding to each concentration are presented in Figures 8a-d.

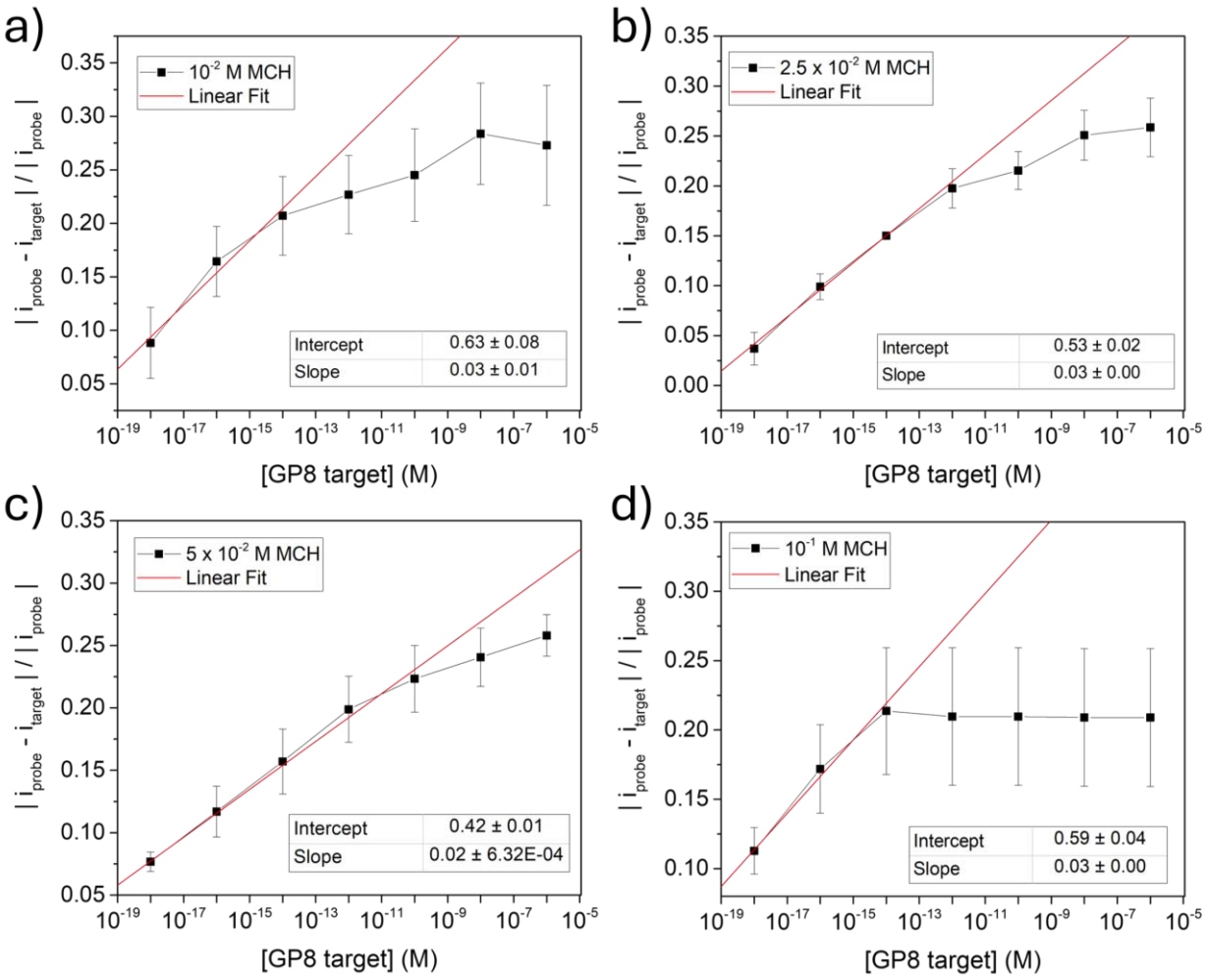

Figure 8. Calibration curves at different concentrations of MCH. a) MCH at 10^{-2} M, b) MCH at $2.5 \cdot 10^{-2}$ M, c) MCH at $5 \cdot 10^{-2}$ M, d) MCH at 10^{-1} M. Each point corresponds to 4 measurements (n=4). Standard errors were calculated by dividing the standard deviation by the square root of n.

Figure 8a presents the hybridization calibration curve for a concentration of 10^{-2} M MCH, *i.e.* a ratio 1:10000 (DNA: MCH). At low concentration, the curve has a linear part. Beyond 10^{-14} M, the curve reaches a plateau, the latter signifying the beginning of saturation of the surface. The same trends were obtained with higher MCH concentrations, the curve reaching the plateau from 10^{-12} M for an MCH concentration at $2.5 \cdot 10^{-2}$ M (Figure 8b), and a plateau from 10^{-10} M for an MCH concentration of $5 \cdot 10^{-2}$ M (Figure 8). Figure 8d presents the hybridization calibration curve for a concentration of 10^{-1} M MCH. We notice that the curve quickly reaches

a plateau, which indicates the faster saturation of the surface. In particular, we hypothesize that at lower MCH concentration 10^{-2} M, and $2.5 \cdot 10^{-2}$ M (Figures 8a and b respectively), the number of MCH molecules attaching to the platinum surface is insufficient to optimally orient ssDNA probes, allowing for easier hybridization of the GP8 target. On the other hand, at higher MCH concentration, 10^{-1} M, the platinum surface became quickly saturated with MCH, resulting in a reduced number of ssDNA probes available on the surface, which limits target detection at 10^{-14} M. As a consequence, the concentration of MCH at $5 \cdot 10^{-2}$M (Figure 8c) is selected as the optimal concentration, as it covers a wider linear dynamic range, and represents a suitable compromise between the cases described above.

Figure 9 compares the detection of target DNA to probe DNA for the two different cases: with and without introduction of MCH. The results are presented in the form of calibration curves. We notice that the two curves are easily distinguishable. In the case of the introduction of MCH (black curve), the curve increases with the increase in the concentration of complementary targets, which means the increase in the surface coverage of the electrode by the target DNAs and therefore of the hybridization. On the other hand, in the opposite case (without introduction of MCH), no hybridization (or even very weak) takes place between the probe and the target, resulting in little to no change in current (red curve), regardless of the target concentrations injected into the chip. The non-oriented adsorption of nucleic acids on platinum and graphite ultramicroelectrodes has been observed in the literature[37]. This highlights the differences in DNA immobilization on gold and platinum surfaces due to the strong affinity of adenine to platinum electrodes, showing that MCH is essential for platinum to prevent planar adsorption of nucleic acid sequences[34].

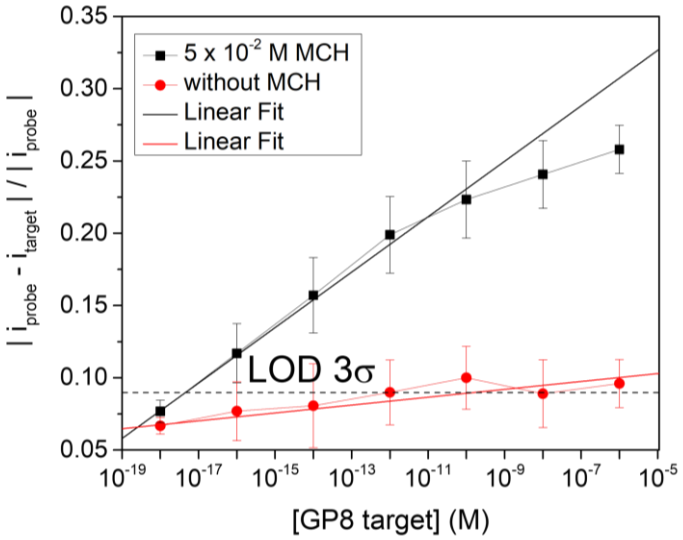

Figure 9. Calibration curves corresponding to DNA hybridization with (black curve) with the optimal concentration ($5 \cdot 10^{-2}$ M) and without the introduction of MCH (red curve). Each point corresponds to 5 measurements (n=5). Standard errors were calculated by dividing the standard deviation by the square root of n. The limit of detection (LOD 3σ) was obtained by multiplying the standard deviation of the lowest concentration by 3.

Calibration and specificity test using the optimal TCEP and MCH ratio

Target DNA detection was monitored using cyclic voltammetry by successive additions of increasing concentrations of the complementary DNA solution (Figure 10a). Each additional grafting step leads to a further decrease in the current density of the redox signal, reflecting an increase in the number of hybridized DNA strands. The progressive reduction of the redox signal thus confirms the effective hybridization of DNA on the modified surface. The fabricated DNA sensor has an excellent detection limit of $1 \cdot 10^{-17}$ M and a wide linear dynamic range from 10^{-18} – 10^{-10} M (Figure 10b). This is comparable to the existing nucleic acid biosensors in the literature as demonstrated in Table 2.

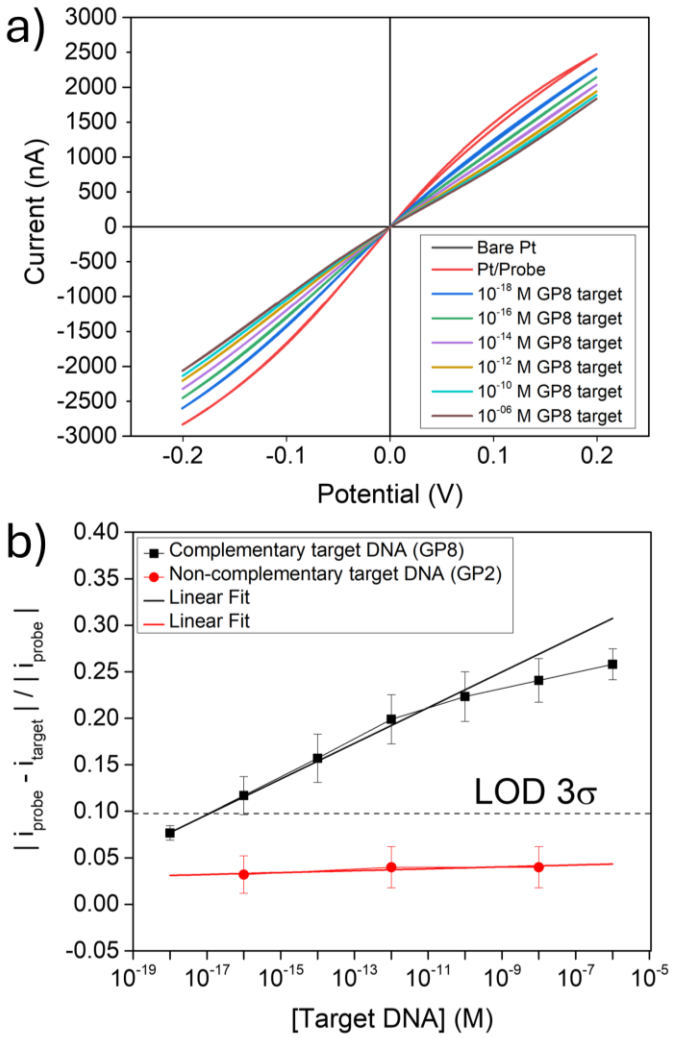

Figure 10. **a)** Monitoring DNA hybridization by cyclic voltammetry. **b)** Calibration curve of a target sequence complementary to the GP8 probe sequence (black curve) compared to the calibration curve for a GP2 target sequence non-complementary to the probe (red curve). Each point corresponds to 4 experiments. The limit of detection (LOD 3σ) was obtained by multiplying the standard deviation of the lowest concentration by 3.

Furthermore, to verify the specificity of the optimized sensor, we also monitored the detection of non-complementary (NC) sequences at three different target DNA concentrations: 10^{-16} M, 10^{-12} M and 10^{-8} M. The results are presented in Figure 10b. The calibration curve of the hybridization of the NC strands remains stable in the background, this confirms that no

hybridization between the probe and the NC target occurs. showing the high specificity of our developed and eoptimized DNA sensor.

Table 2. Comparison of assays performances with existing electrochemical nucleic acid biosensors in the literature.

Electrochemical set-up	LOD	Type of capture target	Reference
Au (3-electrode), EIS	$1 \cdot 10^{-14}$ M	27-base DNA	[38]
Au (3-electrode), CV	$1.7 \cdot 10^{-16}$ M	22-base miRNA	[39]
Au UMEs (2-electrode), CV	$1 \cdot 10^{-16}$ M	21-base miRNA	[13]
Al-IDE (2-electrode), EIS	$1 \cdot 10^{-17}$ M	28-base DNA	[40]
Au (2-electrodes), CV	$1 \cdot 10^{-14}$ M	21-base miRNA	[23]
Au (2-electrodes) on Chip, CV	$1 \cdot 10^{-16}$ M	21-base miRNA	[14]
C amorphous carbon nitride (2-electrodes) on Chip, EIS	$1 \cdot 10^{-18}$ M	21-base miRNA	[6]
Pt (2-electrodes) on Chip, CV	$1 \cdot 10^{-17}$ M	23-base DNA	This work

Conclusions

In this paper, we offer significant insights into the optimization of thiolated oligonucleotide immobilization on platinum electrodes in microfluidic platforms. We identified optimal concentrations of TCEP and MCH (5 mM and 50 mM, respectively) which significantly enhanced DNA probe attachment and orientation on the electrode surface. This optimization leads to a more compact DNA monolayer, maximizing surface coverage and facilitating more effective target hybridization. Using this approach, we successfully detected complementary DNA concentrations within 30 minutes, with a detection limit of 10^{-17} M. Additionally, the use of platinum electrodes proves advantageous due to their electrochemical stability and reduced non-specific adsorption.

Our device currently cannot be reused after each measurement due to the persistent attachment of target DNA to the sensor surface. In this context, we envisage the future development of a comprehensive protocol for effective DNA denaturation to provide reusability. By enabling the removal of bound DNA targets following each measurement, the sensor could be reused for subsequent analyses. However, achieving consistent and complete denaturation without compromising the integrity of the sensor surface presents a considerable challenge, as it necessitates meticulous control over the chemical or thermal conditions.

Nonetheless, our findings not only advance the understanding of oligonucleotide immobilization but also help further future development in microfluidic biosensing technologies, with potential applications in nucleic acid bioanalysis and diagnostics.

AUTHOR INFORMATION

Corresponding Author

Jean Gamby – Team Smart Biosystems, MicroNanoBioFluidics department, UMR 9001 - Centre de Nanosciences et de Nanotechnologies (C2N), CNRS, Université Paris-Saclay, Université Paris Cité, 10 boulevard Thomas Gobert, 91120 Palaiseau, France.

orcid.org/0000-0001-7613-8872

Email: jean.gamby@cnrs.fr

Authors

Choayb Omar – Team Smart Biosystems, MicroNanoBioFluidics department, UMR 9001 - Centre de Nanosciences et de Nanotechnologies (C2N), CNRS, Université Paris-Saclay, Université Paris Cité, 10 boulevard Thomas Gobert, 91120 Palaiseau, France.

Martina Freisa – Team Smart Biosystems, MicroNanoBioFluidics department, UMR 9001 - Centre de Nanosciences et de Nanotechnologies (C2N), CNRS, Université Paris-Saclay, Université Paris Cité, 10 boulevard Thomas Gobert, 91120 Palaiseau, France.

Hiu Mun Man – Team Smart Biosystems, MicroNanoBioFluidics department, UMR 9001 - Centre de Nanosciences et de Nanotechnologies (C2N), CNRS, Université Paris-Saclay, Université Paris Cité, 10 boulevard Thomas Gobert, 91120 Palaiseau, France.

Djamila Kechkeche – Team Smart Biosystems, MicroNanoBioFluidics department, UMR 9001 - Centre de Nanosciences et de Nanotechnologies (C2N), CNRS, Université Paris-Saclay, Université Paris Cité, 10 boulevard Thomas Gobert, 91120 Palaiseau, France.

Thi Hong Nhung Dinh – Team Smart Biosystems, MicroNanoBioFluidics department, UMR 9001 - Centre de Nanosciences et de Nanotechnologies (C2N), CNRS, Université Paris-Saclay, Université Paris Cité, 10 boulevard Thomas Gobert, 91120 Palaiseau, France.

Anne-Marie Haghiri-Gosnet – Team Smart Biosystems, MicroNanoBioFluidics department, UMR 9001 - Centre de Nanosciences et de Nanotechnologies (C2N), CNRS, Université Paris-Saclay, Université Paris Cité, 10 boulevard Thomas Gobert, 91120 Palaiseau, France.

Isabelle Le Potier – Team Smart Biosystems, MicroNanoBioFluidics department, UMR 9001 - Centre de Nanosciences et de Nanotechnologies (C2N), CNRS, Université Paris-Saclay, Université Paris Cité, 10 boulevard Thomas Gobert, 91120 Palaiseau, France.

ACKNOWLEDGMENTS

The authors thank the DIMELEC project ANR-19-CE09-0016 for funding and RENATECH clean room facilities at C2N, Palaiseau, France. C.O. and M.F. thank the doctoral school "Electrical, Optical, Bio-Physics and Engineering" (ED575) and Paris-Saclay University for PhD grants. The authors are also grateful to Professor H. Jacquier (Hôpital Henri Mondor, APHP, Créteil, France) for fruitful discussions concerning the choice of synthetic GP8 and GP2 sequences.

REFERENCES

(1) Liu, A.; Wang, K.; Weng, S.; Lei, Y.; Lin, L.; Chen, W.; Lin, X.; Chen, Y. Development of Electrochemical DNA Biosensors. *TrAC Trends in Analytical Chemistry* **2012**, *37*, 101–111. https://doi.org/10.1016/j.trac.2012.03.008.

(2) Clack, N. G.; Salaita, K.; Groves, J. T. Electrostatic Readout of DNA Microarrays with Charged Microspheres. *Nat Biotechnol* **2008**, *26* (7), 825–830. https://doi.org/10.1038/nbt1416.

(3) Furst, A. L.; Hill, M. G.; Barton, J. K. DNA-Modified Electrodes Fabricated Using Copper-Free Click Chemistry for Enhanced Protein Detection. *Langmuir* **2013**, *29* (52), 16141–16149. https://doi.org/10.1021/la403262v.

(4) Rashid, J. I. A.; Yusof, N. A. The Strategies of DNA Immobilization and Hybridization Detection Mechanism in the Construction of Electrochemical DNA Sensor: A Review. *Sensing and Bio-Sensing Research* **2017**, *16*, 19–31. https://doi.org/10.1016/j.sbsr.2017.09.001.

(5) Liu, S.; Zheng, Z.; Li, X. Advances in Pesticide Biosensors: Current Status, Challenges, and Future Perspectives. *Anal Bioanal Chem* **2013**, *405* (1), 63–90. https://doi.org/10.1007/s00216-012-6299-6.

(6) Horny, M.-C.; Dupuis, V.; Siaugue, J.-M.; Gamby, J. Release and Detection of microRNA by Combining Magnetic Hyperthermia and Electrochemistry Modules on a Microfluidic Chip. *Sensors* **2021**, *21* (1), 185. https://doi.org/10.3390/s21010185.

(7) Drummond, T. G.; Hill, M. G.; Barton, J. K. Electrochemical DNA Sensors. *Nat Biotechnol* **2003**, *21* (10), 1192–1199. https://doi.org/10.1038/nbt873.

(8) Campos, R.; Kotlyar, A.; Ferapontova, E. E. DNA-Mediated Electron Transfer in DNA Duplexes Tethered to Gold Electrodes via Phosphorothioated dA Tags. *Langmuir* **2014**, *30* (40), 11853–11857. https://doi.org/10.1021/la502766g.

(9) Velusamy, V.; Arshak, K.; Yang, C. F.; Yu, L.; Korostynska, O.; Adley, C. Comparison between DNA Immobilization Techniques on a Redox Polymer Matrix. *American Journal of Analytical Chemistry* **2011**, *2* (3), 392–400. https://doi.org/10.4236/ajac.2011.23048.

(10) Amouzadeh Tabrizi, M.; Shamsipur, M. A Label-Free Electrochemical DNA Biosensor Based on Covalent Immobilization of Salmonella DNA Sequences on the Nanoporous Glassy Carbon Electrode. *Biosensors and Bioelectronics* **2015**, *69*, 100–105. https://doi.org/10.1016/j.bios.2015.02.024.

(11) Gamby, J.; Lazerges, M.; Girault, H. H.; Deslouis, C.; Gabrielli, C.; Perrot, H.; Tribollet, B. Electroacoustic Polymer Microchip as an Alternative to Quartz Crystal Microbalance for Biosensor Development. *Anal. Chem.* **2008**, *80* (23), 8900–8907. https://doi.org/10.1021/ac800443u.

(12) Steichen, M.; Brouette, N.; Buess-Herman, C.; Fragneto, G.; Sferrazza, M. Interfacial Behavior of a Hairpin DNA Probe Immobilized on Gold Surfaces. *Langmuir* **2009**, *25* (7), 4162–4167. https://doi.org/10.1021/la802834a.

(13) Horny, M.-C.; Lazerges, M.; Siaugue, J.-M.; Pallandre, A.; Rose, D.; Bedioui, F.; Deslouis, C.; Haghiri-Gosnet, A.-M.; Gamby, J. Electrochemical DNA Biosensors Based on Long-Range Electron Transfer: Investigating the Efficiency of a Fluidic Channel Microelectrode Compared to an Ultramicroelectrode in a Two-Electrode Setup. *Lab Chip* **2016**, *16* (22), 4373–4381. https://doi.org/10.1039/C6LC00869K.

(14) Poujouly, C.; Le Gall, J.; Freisa, M.; Kechkeche, D.; Bouville, D.; Khemir, J.; Gonzalez-Losada, P.; Gamby, J. Microfluidic Chip for the Electrochemical Detection of MicroRNAs: Methylene Blue Increasing the Specificity of the Biosensor. *Front. Chem.* **2022**, *10*. https://doi.org/10.3389/fchem.2022.868909.

(15) Lee, S.; Kim, W. J.; Chung, M. Enhanced Electrochemical Biosensing on Gold Electrodes with a Ferri/Ferrocyanide Redox Couple. *Analyst* **2021**, *146* (17), 5236–5244. https://doi.org/10.1039/D1AN00952D.
(16) Zhou, W.; Ding, J.; Liu, J. A Platinum Shell for Ultraslow Ligand Exchange: Unmodified DNA Adsorbing More Stably on Platinum than Thiol and Dithiol on Gold. *Chem. Commun.* **2015**, *51* (60), 12084–12087. https://doi.org/10.1039/C5CC04340A.
(17) Yu, H.; Yu, J.; Li, L.; Zhang, Y.; Xin, S.; Ni, X.; Sun, Y.; Song, K. Recent Progress of the Practical Applications of the Platinum Nanoparticle-Based Electrochemistry Biosensors. *Front. Chem.* **2021**, *9*. https://doi.org/10.3389/fchem.2021.677876.
(18) Melnikova, D. L.; Skirda, V. D.; Nesmelova, I. V. Effect of Reducing Agent TCEP on Translational Diffusion and Supramolecular Assembly in Aqueous Solutions of α-Casein. *J. Phys. Chem. B* **2019**, *123* (10), 2305–2315. https://doi.org/10.1021/acs.jpcb.8b12511.
(19) Wang, Y.; Chen, X.; Xu, X.; Du, M.; Wu, C. Reducing Disulfide Bonds as a Robust Strategy to Facilitate the Self-Assembly of Cod Protein Fabricating Potential Active Ingredients-Nanocarrier. *Colloids Surf B Biointerfaces* **2023**, *222*, 113080. https://doi.org/10.1016/j.colsurfb.2022.113080.
(20) Avershina, E.; Khezri, A.; Ahmad, R. Clinical Diagnostics of Bacterial Infections and Their Resistance to Antibiotics—Current State and Whole Genome Sequencing Implementation Perspectives. *Antibiotics* **2023**, *12* (4), 781. https://doi.org/10.3390/antibiotics12040781.
(21) Rivoarilala, O. L.; Garin, B.; Andriamahery, F.; Collard, J. M. Rapid in Vitro Detection of CTX-M Groups 1, 2, 8, 9 Resistance Genes by LAMP Assays. *PLOS ONE* **2018**, *13* (7), e0200421. https://doi.org/10.1371/journal.pone.0200421.
(22) Shurina, B. A.; Page, R. C. Structural Comparisons of Cefotaximase (CTX-M-Ase) Sub Family 1. *Front. Microbiol.* **2021**, *12*. https://doi.org/10.3389/fmicb.2021.688509.
(23) Lazerges, M.; Tal, V. T.; Bigey, P.; Scherman, D.; Bedioui, F. Electrochemical DNA-Biosensors: Two-Electrode Setup Well Adapted for Miniaturized Devices. *Sensors and Actuators B: Chemical* **2013**, *182*, 510–513. https://doi.org/10.1016/j.snb.2013.02.098.
(24) Poujouly, C.; Gonzalez-Losada, P.; Boukraa, R.; Freisa, M.; Le Gall, J.; Bouville, D.; Deslouis, C.; Gamby, J. Diffusion–Convection Impedance for a Micro-Band Electrode under Microfluidic Conditions. *Electrochemistry Communications* **2022**, *137*, 107262. https://doi.org/10.1016/j.elecom.2022.107262.
(25) Poujouly, C. Plateforme Microfluidique Pour La Détection Électrochimique Multiplexée de microARNs Du Cancer. These de doctorat, université Paris-Saclay, 2022. https://theses.fr/2022UPAST062 (accessed 2024-11-13).
(26) Horny, M.-C.; Freisa, M.; Poujouly, C.; Gonzalez-Losada, P.; Le Gall, J.; Dinh, T.-H.-N.; Bouville, D.; Le Potier, I.; Pallandre, A.; Gamby, J. Electrochemical Nucleic Acid Biosensor on a Microfluidic Chip to Understand the Coupling between Electrochemistry and Microfluidics. *J. Chem. Educ.* **2024**, *101* (2), 605–611. https://doi.org/10.1021/acs.jchemed.3c01054.
(27) Burns, J. A.; Butler, J. C.; Moran, J.; Whitesides, G. M. Selective Reduction of Disulfides by Tris(2-Carboxyethyl)Phosphine. *J. Org. Chem.* **1991**, *56* (8), 2648–2650. https://doi.org/10.1021/jo00008a014.
(28) Qing, Z.; Luo, G.; Xing, S.; Zou, Z.; Lei, Y.; Liu, J.; Yang, R. Pt-S Bond-Mediated Nanoflares for High-Fidelity Intracellular Applications by Avoiding Thiol Cleavage. *Angew Chem Int Ed Engl* **2020**, *59* (33), 14044–14048. https://doi.org/10.1002/anie.202003964.
(29) Yang, B.; Agrios, A. G. Attachment of Pt Nanoparticles to a Metal Oxide Surface Using a Thiol–Carboxyl Bifunctional Molecule. *Journal of Colloid and Interface Science* **2018**, *513*, 464–469. https://doi.org/10.1016/j.jcis.2017.11.058.

(30) Steel, A. B.; Herne, T. M.; Tarlov, M. J. Electrochemical Quantitation of DNA Immobilized on Gold. *Anal. Chem.* **1998**, *70* (22), 4670–4677. https://doi.org/10.1021/ac980037q.
(31) Sun, B.; Colavita, P. E.; Kim, H.; Lockett, M.; Marcus, M. S.; Smith, L. M.; Hamers, R. J. Covalent Photochemical Functionalization of Amorphous Carbon Thin Films for Integrated Real-Time Biosensing. *Langmuir* **2006**, *22* (23), 9598–9605. https://doi.org/10.1021/la061749b.
(32) Konopka, S. J.; McDuffie, Bruce. Diffusion Coefficients of Ferri- and Ferrocyanide Ions in Aqueous Media, Using Twin-Electrode Thin-Layer Electrochemistry. *Anal. Chem.* **1970**, *42* (14), 1741–1746. https://doi.org/10.1021/ac50160a042.
(33) Kelley, S. O.; Boon, E. M.; Barton, J. K.; Jackson, N. M.; Hill, M. G. Single-Base Mismatch Detection Based on Charge Transduction through DNA. *Nucleic Acids Research* **1999**, *27* (24), 4830–4837. https://doi.org/10.1093/nar/27.24.4830.
(34) Freisa, M.; Poujouly, C.; Le Potier, I.; Dinh, T. H. N.; Couraud, L.; Bouville, D.; Sella, C.; Thouin, L.; Gamby, J. Highlighting the Impact of Blocking Monolayers on DNA Electrochemical Sensors. Theoretical and Experimental Investigations under Flow Conditions. *Electrochimica Acta* **2024**, *505*, 145006. https://doi.org/10.1016/j.electacta.2024.145006.
(35) Armbruster, M. H.; Austin, J. B. The Adsorption of Gases on Plane Surfaces of Mica. *J. Am. Chem. Soc.* **1938**, *60* (2), 467–475. https://doi.org/10.1021/ja01269a066.
(36) Lin, Z.; Strother, T.; Cai, W.; Cao, X.; Smith, L. M.; Hamers, R. J. DNA Attachment and Hybridization at the Silicon (100) Surface. *Langmuir* **2002**, *18* (3), 788–796. https://doi.org/10.1021/la010892w.
(37) Basu, N.; Ho, T. H.; Guillon, F.-X.; Zhang, Y.; Bigey, P.; Navakanta, B.; Bedioui, F.; Lazerges, M. Coupling Electrochemical Adsorption and Long-Range Electron Transfer: Label-Free DNA Mismatch Detection with Ultramicroelectrode (UME). *Electroanalysis* **2019**, *31* (11), 2232–2237. https://doi.org/10.1002/elan.201900357.
(38) Hassen, W. M.; Chaix, C.; Abdelghani, A.; Bessueille, F.; Leonard, D.; Jaffrezic-Renault, N. An Impedimetric DNA Sensor Based on Functionalized Magnetic Nanoparticles for HIV and HBV Detection. *Sensors and Actuators B: Chemical* **2008**, *134*, 755–760. https://doi.org/10.1016/j.snb.2008.06.020.
(39) Chandra, S.; Adeloju, S. A New Sensor for Detecting Microrna 133B (Parkinson's Disease Biomarker). *Sensors International* **2020**, *1*, 100005. https://doi.org/10.1016/j.sintl.2020.100005.
(40) Cheng, C.; Oueslati, R.; Wu, J.; Chen, J.; Eda, S. Capacitive DNA Sensor for Rapid and Sensitive Detection of Whole Genome Human Herpesvirus-1 dsDNA in Serum. *Electrophoresis* **2017**, *38* (12), 1617–1623. https://doi.org/10.1002/elps.201700043.

Graphical abstract